EurJIC
European Journal of Inorganic Chemistry

Research Article
doi.org/10.1002/ejic.202300668

Chemistry Europe
European Chemical Societies Publishing

www.eurjic.org

Modified Gold Nanoparticles Modulated Fluorescence and Singlet Oxygen Generation of Pheophorbide *a* as an Effective Platform for Photodynamic Therapy against *Staphylococcus aureus*

Daniel Ziental,[a] Paulina Błaszkiewicz,[b, c] Jolanta Długaszewska,[d] Emre Güzel,[e] Alina Dudkowiak,[b] and Lukasz Sobotta*[a]

Dedicated to Professor Tomás Torres on the occasion of his 70th birthday

The paper reports on the synthesis and evaluation of photochemical properties of gold nanorods (Au–NRs) coated with PEG with a thiol (–SH) group or SiO_2 and their physical mixtures with pheophorbide *a*. Also biological activity of these systems was tested in photodynamic therapy directed towards *Staphylococcus aureus*. The potential additive effect between differently functionalized Au–NRs and the dye pheophorbide *a* was also studied. The efficiency of singlet oxygen generation varied considerably depending on the type of PEG polymer used for coating NRs and was the highest, of 65%, for the polymer PEG (10k) and the Au–NRs concentration of (1.33×10^{-11} M). For the other studied PEGs (2k, 5k) and the same concentration of NRs, a decrease in the singlet oxygen generation efficiency was observed. The most effective against Gram-positive bacteria were the mixtures of PEG-coated Au–NRs with pheophorbide *a*, exposed to irradiation at 405 nm and 660 nm, which provided a >5.8 log reduction in the bacteria growth. However, no strong bactericidal effect was noted in the case of irradiation with 525 nm.

Introduction

Photodynamic therapy (PDT) has emerged as a valuable therapeutic option for combating bacterial, fungal, and viral infections, however, it has some limitations when applied to the disease affected tissues.[1–7] The inherent limitations of the standard photosensitizer (PS) formulations can be eliminated or reduced by physically encapsulating PSs into nanocarriers.[8–10] Under physiological conditions, transport of hydrophobic PSs to target sites may be facilitated when they are encapsulated into stable formulations such as polymeric nanocarriers which should have the optimal size for prolonged circulation in the organisms. In recent years, many different drug delivery systems have been developed. An example of the most promising ones is the conjugation of PS with gold nanoparticles (Au–NPs) platform, leading to the formation of water-soluble systems with efficient singlet oxygen generation (ϕ_Δ).[11,12]

Au–NPs offer several benefits as PS delivery systems, including protection of the PS from enzymatic degradation, control of PS release to ensure constant and uniform concentration in target cells and the ability to penetrate target cells thanks to their submicron size, biocompatibility and resorbability through natural pathways.

Suitable functionalization minimizes the problems associated with nanoparticle aggregation, stability, and toxicity in relation to living organisms.[13] Many synthetic polymers have been used to enhance the biocompatibility of gold nanorods (Au–NRs). However, polyethylene glycol (PEG) is the most popular.[14,15] PEG is widely known for its biocompatibility, its stealth properties, resistance to protein adsorption, and its extended circulation time in the plasma.[8]

In recent years, numerous modifications of Au–NPs have been developed to enhance their antimicrobial potential. Au–NPs have been linked to antibiotics, phospholipids, and polymers, among others.[16] Development of new gold-based platforms for photodynamic antimicrobial chemotherapy (PACT) is currently underway. Rossi *et al.* have developed a polyurethane-based matrix with anchored Au–NRs and a dye (crystal violet – CV). The system was exposed to white light and, as a result, it was able to reduce the number of colony-forming units (CFU) of *E. coli* bacteria by up to 99% (2 log).[17] It is assumed that the increased efficacy of PDT using nanospheres

[a] D. Ziental, L. Sobotta
Chair and Department of Inorganic and Analytical Chemistry, Poznan University of Medical Sciences, Rokietnicka 3, 60-806 Poznan, Poland
E-mail: lsobotta@ump.edu.pl

[b] P. Błaszkiewicz, A. Dudkowiak
Faculty of Materials Engineering and Technical Physics, Poznan University of Technology, Piotrowo 3, 60-965 Poznan, Poland

[c] P. Błaszkiewicz
NanoBioMedical Centre, Adam Mickiewicz University, Wszechnicy Piastowskiej 3, 61-614 Poznan, Poland

[d] J. Długaszewska
Chair and Department of Genetics and Pharmaceutical Microbiology, Poznan University of Medical Sciences, Rokietnicka 3, 60-806 Poznan, Poland

[e] E. Güzel
Department of Engineering Fundamental Sciences, Sakarya University of Applied Sciences, 54050 Sakarya, Türkiye

(Au–NSs) and Au–NRs may be related to their higher absorption coefficient than those of organic dyes.[18] In another study, gold nanoclusters in combination with CV have been used, leading after irradiation, to a reduction in the number of viable *S. aureus* bacteria by more than 3.3 logs.[19] Au–NSs were combined with methylene blue (MB) to study photodynamic activity and then tested against planktonic *S. mutans* and its biofilm. The experiment showed that both Au–NPs–MB combinations and MB alone were effective against the bacteria, but there was no significant difference in effectiveness between them.[20] A different conclusion was reached by Maliszewska *et al.*, who demonstrated greater effectiveness of biogenic Au–NSs in combination with MB. In this case, a better effect was achieved for both Gram-positive *S. aureus* and Gram-negative *E. coli*.

Moreover, the combination with biogenic Au–NSs partially prevented the photobleaching effect and increased the effectiveness of PACT.[21] Rahme *et al.* have synthesized Au–NSs with diameters ranging from 15 to 170 nm. PEG polymers with a thiol group (PEG–SH), of molecular mass in the range from 2100 to 51000 g mol^{-1} were used as effective ligands to stabilize the molecules.[22] Cheng *et al.* have developed a highly efficient drug vector for PDT by synthesizing Au–NSs with PEG–SH conjugates, which act as a water-soluble, biocompatible 'cage' to deliver a hydrophobic drug to the PDT site of action. They demonstrated that the drug release dynamics *in vitro* in a biphasic solution system and *in vivo* in cancer-bearing mice indicated that drug delivery was highly efficient, and that passive targeting favored the tumor site. In the case of Au–NSs and silicon phthalocyanine conjugates (Au–NPs@Pc4), the drug delivery time required for PDT was significantly reduced, to less than 2 h, compared to 2 days for the free drugs.[11] An interesting approach has been presented by Hone *et al.* The Au–NSs were stabilized with phthalocyanine (Pc) as a PS. Ternary nanoparticles (PS/Au–NPs/reagent transfer phase) were shown to generate singlet oxygen with increased quantum yields compared to the free Pc.[23] In addition, it has been previously reported that the transfer phase enhances the solubility of the surface-bound hydrophobic PS in polar solvents, which would facilitate their systemic injection. The results suggest that these ternary structures have the potential to be useful carriers for the delivery of PSs in PDT procedures.[8] To confirm the therapeutic efficacy of Au–NRs@PEG–SH physical mixtures, they were tested against bacteria. It was concluded that plasmonic nanoparticles could be delivered to both Gram-positive and Gram-negative bacteria, boosting both the photo-antibacterial activity and the singlet oxygen level in the cells.[24,25]

In this work, we have presented the influence of functionalized Au–NRs and PS in physical mixtures on antimicrobial activity. The photodynamic effect can be controlled by modification of the Au–NRs coating type. Moreover, we have shown that these mixtures can be used as an alternative to antibiotic therapy, due to the efficiency of ϕ_Δ and their photoactivity against Gram-positive *S. aureus*.

Results and discussion

The synthesis of Au–NRs was carried out by a *seed-mediated growth* method. Au–NRs were characterized by UV-Vis spectroscopy and exhibited a characteristic transversal and longitudinal peaks at 520 nm and 660 nm, respectively (Figure 1). The final concentration of Au–NRs was calculated from the Lambert-Beer law. Based on TEM images of NRs, the aspect ratio of 2.25 (the length 53.2 nm ± 1.8 nm and width 23.6 nm ± 1.3 nm) was calculated, and their extinction coefficient was adopted from the work of Orendorff and Murphy.[26] A particularly important problem is the role of silver ion in the synthesis of seed growth. The concentration of silver nitrate is an essential parameter in the control of the aspect ratio of these single crystalline Au–NRs during synthesis. Single-crystal Au–NRs must contain Ag^+ ions, as pentawinned Au–NRs cannot grow anisotropically without them. Metal reduction with Au–NRs tips is less selective in the absence of silver as a surface-active agent.[27] The functionalization process of Au–NRs was carried out using SiO_2 and PEG–SH with different chain lengths (2k, 5k, 10k). Regardless of the type of nanocomposite to be designed, the colloidal stability of the resulting solution and the ease of functionalization are the key factors. A potential desorption of the ligands from Au–NPs is another crucial point. In particular, silica appears to be an excellent choice to prevent particle coalescence and solve this issue. In addition, silica is optically transparent, chemically inert, and easy to functionalize. The tetraethyl orthosilicate (TEOS) was used to functionalize Au–NRs in the first stage of the synthesis. The silane groups completely covered the Au surface resulting in positive contact with the metal by the condensation of siloxane groups (Figure 1). The hydrolysis and condensation of TEOS to form SiO_2 can be catalyzed by changing pH values. For this study, the Au–NRs with a length of 53.2 nm ± 1.8 nm and width 23.6 nm ± 1.3 nm were selected. The thickness of the silica coated was 14 ± 2.4 nm.[28]

On the other hand, the substance most often used for the thiol modification of surface nanoparticles is PEG with a thiol (–SH) group. PEG is a neutral hydrophilic polymer that imparts a high degree of stability and biocompatibility to Au–NRs and gives nanostructures the'stealth' quality. The process of PEGylation is a complex and multi-faceted one, involving a number of physical and chemical processes. The dissolution of the CTAB ligands, the diffusion of the PEG ligands into the CTAB layer, and the reaction or absorption of PEG–SH with gold are all necessary reaction steps for PEGylation.[14,15,29] The general consensus is that plain Au–NRs are toxic *in vitro* as well as *in vivo* depending on the concentration. The toxic effect (such as that of Ag^+) can be reduced or even eliminated by properly modifying the surface of Au–NRs (SiO_2 or PEG–SH). The shell acts as a physical barrier that should minimize interactions with the nanomaterial surface and the release of toxic ions from the core material that could interact with the organisms. To avoid problems such as the irreversible aggregation of Au–NRs, the synthesis settings, and environment must be carefully managed at each stage. Several important variables can have impact on the thickness, the grafting density, and the exchange efficiency of Au–NRs PEGylation. For PEGylation, the Au–NRs with an

Research Article
doi.org/10.1002/ejic.202300668

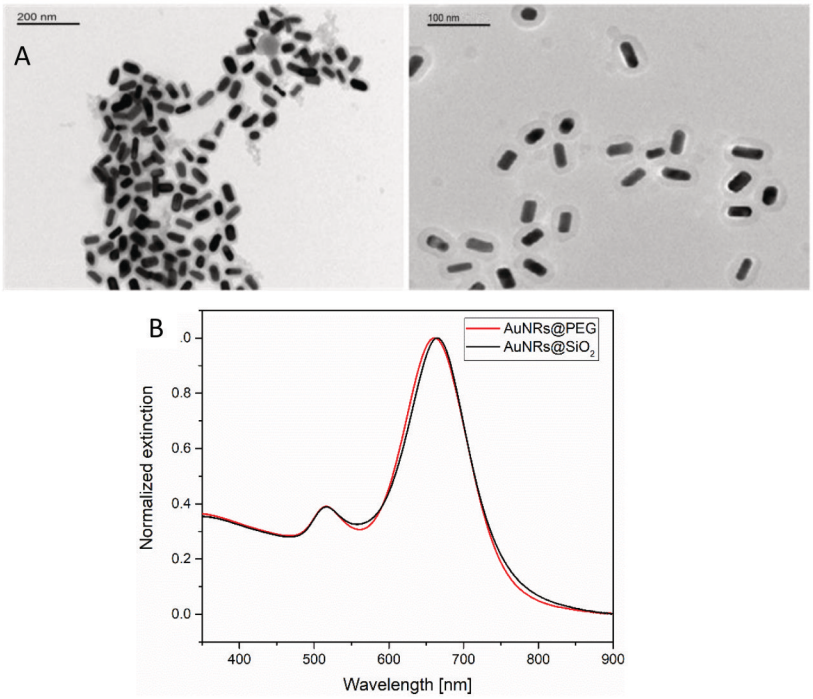

Figure 1. A) TEM images of coated gold nanorods by SiO_2 (Au–NRs@SiO_2); B) extinction spectra of AuNRs@PEG–SH and AuNRs@SiO_2.

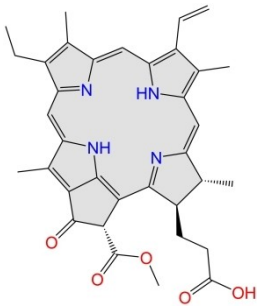

Figure 2. Molecular structure of pheophorbide *a*.

aspect ratio of 2.25 were selected. The details of the functionalization process have been recently presented by Błaszkiewicz *et al.*[28,30] and Tim *et al.*[31] The value of ϕ_Δ is one of the most important photophysical factors. It defines the photodynamic potential and the ability to affect biological structures. As the value of this parameter for the chlorophyll derivative pheophorbide *a* (Pheide *a*, Figure 2) (the product of the decomposition of chlorophyll occurring in nature) is about 62% (EtOH),[32] it was chosen for the study. A series of physical mixtures containing a constant concentration of the dye and a variable concentration of the Au–NRs, was prepared. Figure 3 shows the dependence of the absorbance on the wavelength of the

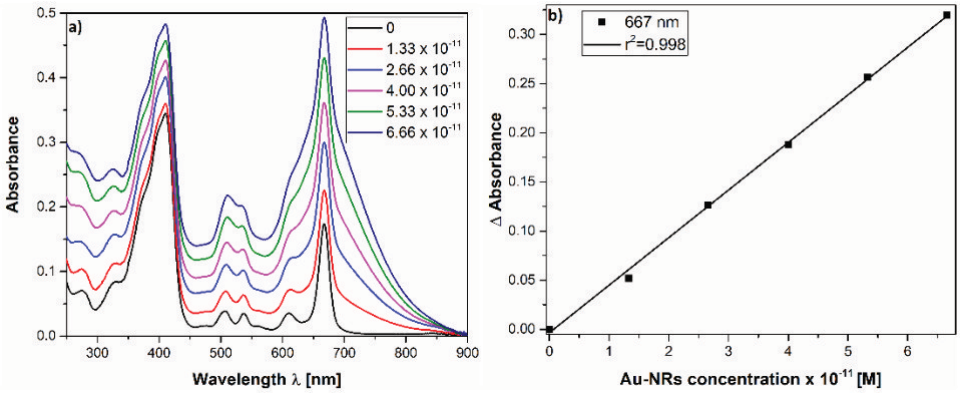

Figure 3. a) Absorption spectra of physical mixtures of Pheide *a* (constant concentration $1.65 \cdot 10^{-6}$ M) with different concentrations of Au–NRs@PEG–SH (10k; (0, 1.33, 2.66, 4.00, 5.33, 6.66)$\cdot 10^{-11}$ M), b) Linear dependence of absorbance on Au–NRs@PEG–SH concentration for a longitudinal maximum of Au–NRs.

Research Article
doi.org/10.1002/ejic.202300668

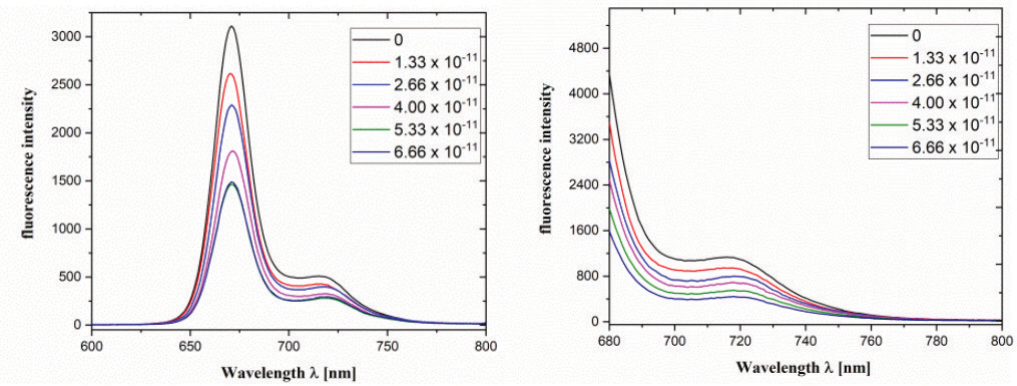

Figure 4. Fluorescence spectra of physical mixtures consisting of Pheide *a* with different contents of Au–NRs@PEG–SH (10k) after excitation at wavelengths of 410 nm (left) and 667 nm (right); the concentration of Pheide *a* was adjusted to $1.65 \cdot 10^{-6}$ M.

absorption spectrum of the prepared physical mixtures. The absorption spectra (not shown) were also recorded for the investigated systems with 1,3-diphenylobensofuran (DPBF) to estimate their efficiency of the singlet oxygen generation.

The increase in the intensity of the absorption band is the result of increasing concentration of Au–NRs in each successive mixture. The stock solutions of Pheide *a* were prepared in such a way that the value of the absorbance at the wavelength corresponding to the Q-band maximum was below 0.15. The absorption spectra of the mixtures studied are characterized by two distinct bands, one at 410 nm and the other at 667 nm. These maxima are related to the Soret and Q bands, respectively, and are due to the presence of Pheide *a*.

The physical mixtures of Au–NRs@PEG–SH – Pheide *a* were subjected to fluorescence analysis, while for the physical mixtures of Au–NRs@SiO_2 – Pheide *a* the data concerning the spectral properties as well as ϕ_Δ based on our previous study, were used.[28] Figure 4 shows the fluorescence spectra of Pheide *a* in the physical mixtures excited at the wavelengths of 410 and 667 nm. The decreasing intensity of the fluorescence bands is correlated with the increase in the concentration of Au–NRs in each successive mixture (Figure 5). The fluorescence efficiency of Pheide *a* for selected concentrations of Au–NRs@PEG–SH (10k; (0, 1.33, 4.00, 6.66)$\cdot 10^{-11}$ M) was calculated and the values are given in Table 1. As can be seen from the data, the fluorescence efficiency of the dye decreases linearly with increasing concentration of Au–NRs (Figure 5).

The Stern-Volmer dependence (Figure 6) was also plotted for the investigated mixtures ((0, 1.33, 4.00, 6.66)$\cdot 10^{-11}$ M). Its linear character suggests a single quenching mechanism and its dynamic character in the studied systems. The K_{SV} values obtained are of the order of 10^{11} M^{-1}. Therefore, the quenching phenomenon may be referred to as 'super quenching'.

The quantum efficiency of ϕ_Δ for the physical mixtures studied, plotted as a function of Au–NRs@PEG–SH concentration (Figure 7), shows that the highest value was obtained for the concentration of $1.33 \cdot 10^{-11}$ M, independently of the

Table 1. Fluorescence efficiency of Pheide *a* in the presence of Au–NRs@PEG–SH (10k) at different concentrations.

Au–NRs@PEG–SH [M]	ϕ_F [%] (410 nm)	ϕ_F [%] (667 nm)
0	28.0	28.0
$1.33 \cdot 10^{-11}$	25.7	26.4
$4.00 \cdot 10^{-11}$	23.9	24.5
$6.66 \cdot 10^{-11}$	20.8	21.6

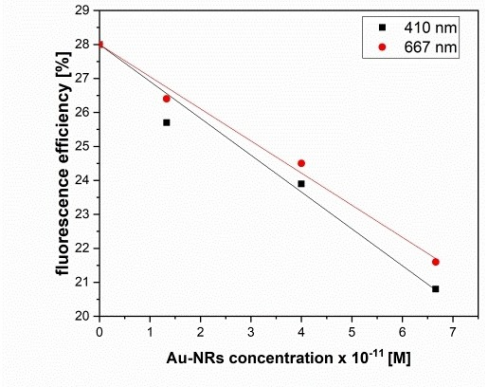

Figure 5. Fluorescence efficiency of Pheide *a* in the presence of Au–NRs@PEG–SH (10k) after excitation at 410 nm and 667 nm.

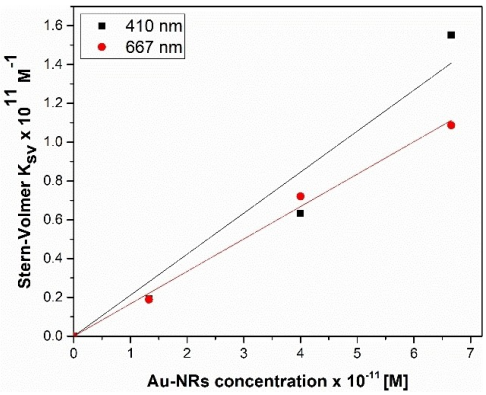

Figure 6. Stern-Volmer dependence of the physical mixtures consisting of Pheide *a* and Au–NRs@PEG–SH (10k) for two excitation wavelengths.

Research Article
doi.org/10.1002/ejic.202300668

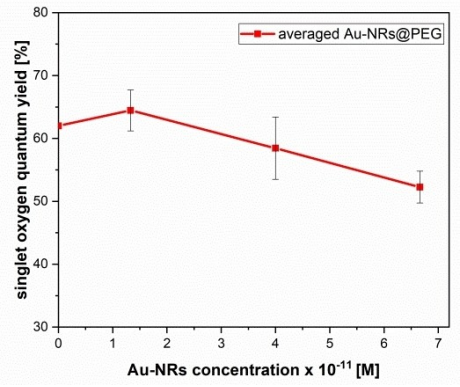

Figure 7. Singlet oxygen generation efficiency for the physical mixtures of Pheide *a* and Au–NRs@PEG–SH (10k) vs. the concentrations of Au–NRs@PEG–SH.

PEG–SH used. For the concentrations higher than the above one, the efficiency decreases significantly, which may be due to the overloading of the nanoparticles and excess polymer chains in the physical mixtures studied.

The type and thickness of the coating layer, the concentration of metal nanostructures and their scattering properties can influence the increase in quantum yield of ϕ_Δ in physical mixtures. Chadwick *et al.*[33] have found that the photogeneration of singlet oxygen with a low quantum yield, is facilitated by citrate-stabilized nanoparticles. This requires careful design of Au–NPs, as even a moderate thickness of the capping layer may completely prevent the formation of singlet oxygen. Furthermore, the efficiency of the process is also dependent on the size of the nanoparticles. Various biocompatible polymers that offer appropriate surface chemistry and stability can be used to coat Au–NRs (e.g. PEG). The coating of the Au–NRs surface with polymers can be a preventive measure against instability, which is a result of aggregation. Previous studies[34] have shown that the PEG coating of Au–NPs affects the efficiency of ϕ_Δ. In addition, the surface charge played an even more important role in regulating the generation of singlet oxygen. It seems that the polymer chain length of (10k) (M_w = 10000) and the obtained thickness of the coating layer formed on NRs by PEG–SH are the most suited for the energy transfer in the investigated systems because the most efficient effect of ϕ_Δ was observed for the mixture of Au–NRs@PEG–SH (10k) – Pheide *a* at the concentrations of $1.33 \cdot 10^{-11}$ M for Au–NRs functionalized with PEG–SH (10k) and $1.65 \cdot 10^{-6}$ M for PS, respectively. The physical mixtures of Au–NRs@PEG–SH (10k) and Pheide *a* were selected for evaluation of biological activity because they showed the highest ϕ_Δ efficiency in comparison with those of PEG–SH (2k) and PEG–SH (5k). The efficiency of singlet oxygen generation in the samples studied was approximately 62% (2k), 63% (5k), and 65% (10k) for the assumed concentration of Au–NRs and different PEG–SH chain lengths of the coating (Table 2). The small difference in ϕ_Δ efficiency between the NRs coated with a polymer of different chain lengths and pure PS may be due to the fact that PEG does not play a significant role in the process of singlet oxygen

Table 2. Quantum yields of singlet oxygen generation for Au–NRs@PEG–SH (2k, 5k, 10k) – Pheide *a* mixtures excited at 667 nm. The concentration of Pheide *a* was adjusted to $1.65 \cdot 10^{-6}$ M and that of Au–NRs@PEG–SH was $1.33 \cdot 10^{-11}$ M.

Type of polymer	ϕ_Δ [%]
2k	62
5k	63
10k	65

generation in the studied systems. A comparison of the results of our earlier studies with the data obtained for Au–NRs@SiO_2,[28] reveals that a better enhancer of singlet oxygen generation is Au–NRs functionalized with the inorganic shell than with PEG–SH.

In our previous work,[28] at a low concentration of Au–NRs ($1.33 \cdot 10^{-11}$ M) and the 14 ± 2.4 nm distance between Au–NRs and the dye molecule (defined by the thickness of the SiO_2 shell), the highest ϕ_Δ efficiency was observed for the physical mixture of Au–NPs@SiO_2 – Pheide *a*. The ϕ_Δ efficiency decreased in the physical mixtures studied with increasing concentration of functionalized Au–NRs.[28] The efficiency of ϕ_Δ in the samples with the dyes coupled with nanoparticles was shown to achieve its maximum value when the distance between the dye and the plasmonic structure was about 10–20 nm, depending on the shape of Au–NPs.[24] It appears that, even in a physical mixture, the distance between the dye and the plasmonic nanoparticles causes increased oxygen production for Au–NRs shell sizes greater than 12 nm. Based on these results, an enhancement factor of ϕ_Δ was estimated to be in the range of 8–11% for Au–NRs@SiO_2 and 0–3% for Au–NRs@PEG–SH. The higher value for the Au–NRs@SiO_2 – Pheide *a* mixture was obtained can be related to the silica acting as a homogenous spacer between the metallic core and PS with simultaneous enhancement of ϕ_Δ.[28] Our results can be compared with those reported by Ke *et al.*[35], who obtained ϕ_Δ enhancement in the hybrid system for the silica thickness of 10.6 nm. In the case of the Au–NRs@PEG–SH – Pheide *a* system, the low yields obtained seem to be related to the thickness and inhomogeneity of the polymer shell.

The first step in evaluation of biological activity was analysis of the antimicrobial activity of the pure dye (Pheide *a*), Au–NRs@SiO_2, and of Au–NRs@PEG–SH. In the second stage, the antimicrobial activity of the Au–NRs–dye physical mixtures was determined. The antimicrobial activity was tested against the Gram-positive bacteria *S. aureus*, which is a medically important pathogen and the cause of many skin and systemic diseases. In the case of particularly susceptible individuals and those with reduced immunity, *S. aureus* infection can lead to irreversible complications and even death.[36] Nosocomial infections with *S. aureus* are often related to post-operative complications.[37] The strain used in the experiment is a reference pathogen for the testing of the activity of antiseptics. Due to the rapid development of resistance in many strains of Gram-positive bacteria, the search for treatments alternative to antibiotics should be a priority for modern medicine.[38–41] In the

Research Article
doi.org/10.1002/ejic.202300668

study carried out, each system was tested upon excitation with light at three characteristic wavelengths, which correspond to the absorption maxima of the ingredients of the system developed. A clear dependence of the photodynamic activity on the wavelength of the excitation irradiation was observed. From among the systems studied, the highest antimicrobial activity was observed for the physical mixture of Au–NRs@PEG–SH with Pheide *a* at the concentrations of $1.33 \cdot 10^{-13}$ M and $1.65 \cdot 10^{-8}$ M, respectively, upon excitation at 660 nm (Figure 8). The bactericidal activity of this mixture exceeded a 5.8 log reduction in bacterial growth (>99.999% reduction). Irradiation at a wavelength of 660 nm is optimal for photodynamic purposes, as it covers the therapeutic window without harming the human body.[42] A slightly lower but still high activity was shown by Pheide *a* (ca. 5 log) and the physical mixtures of Au–NRs@SiO_2 with Pheide *a* at the concentrations of $1.33 \cdot 10^{-13}$ M and $1.65 \cdot 10^{-8}$ M, respectively. The results of this study indicate that these systems may be excellent candidates for medical applications. Importantly, the activity above 4 log reduction in bacterial growth according to Jori *et al.* undoubtedly classified the investigated systems as bactericidal.[43] However, based on previous research, gold's historic and well-documented bacteriostatic and bactericidal effects should be emphasized.[1]

On the other hand, the photodynamic antibacterial effect of the Au–NRs@PEG–SH nanoparticles was not observed. Similarly, no bactericidal effect was observed for Au–NRs@SiO_2 with a lower concentration of NRs after irradiation at 525 nm.

Analyzing the data for the investigated systems irradiated at 405 nm, particular attention should be paid to the increase in toxicity of the medium containing 5% ethanol. It may be related to the previously documented increase in the permeability of the bacterial membrane when exposed to UV light.

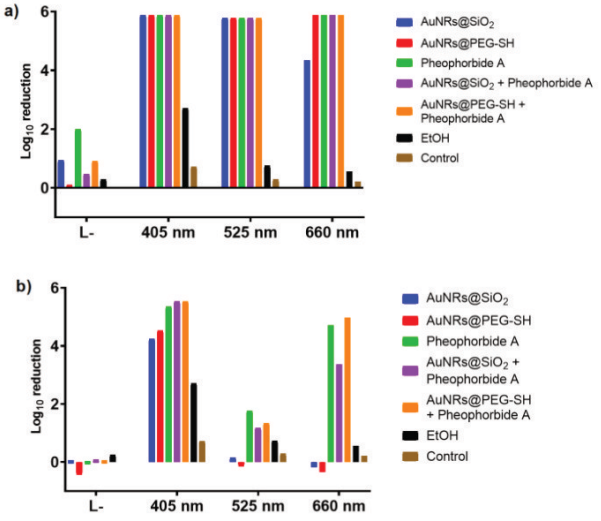

Figure 8. Biological activity of the investigated systems: **a)** Au–NRs@SiO_2 – $6.66 \cdot 10^{-11}$ M; Au–NRs@PEG–SH – $6.66 \cdot 10^{-11}$ M; Pheide *a* – $8.25 \cdot 10^{-8}$ M; Au–NRs@SiO_2 – $6.65 \cdot 10^{-13}$ M in mixture with Pheide *a* – $8.25 \cdot 10^{-8}$ M; Au–NRs@PEG–SH – $6.65 \cdot 10^{-13}$ M in mixture with Pheide *a* – $8.25 \cdot 10^{-8}$ M; ethanol 5% (v/v); **b)** Au–NRs@SiO_2 – $1.2 \cdot 10^{-11}$ M; Au–NRs@PEG–SH – $1.33 \cdot 10^{-13}$ M; Pheide *a* – $1.65 \cdot 10^{-8}$ M; Au–NRs@SiO_2 – $1.33 \cdot 10^{-13}$ M in mixture with Pheide *a* – $1.65 \cdot 10^{-8}$ M; Au–NRs@PEG–SH – $1.33 \cdot 10^{-13}$ M in mixture with Pheide *a* – $1.65 \cdot 10^{-8}$ M; ethanol 1% (v/v). The size of Au–NRs was 53.2 nm ± 1.8 nm (length) and 23.6 nm ± 1.3 nm (width).

The use of light in the near-UV range has been shown to have a negative effect on bacterial growth,[44] but this light can also be potentially harmful to humans after repeated exposure.[45] Therefore, it should be emphasized that the use of PDT mediated by UV-light, whatever its effect, should be reserved for surface disinfection or the development of self-sterilizing materials. In the case of exposure to light at 525 nm, the bactericidal effect of Au–NPs was clearly predominant, which could be due to the lower absorption of Pheide *a* in this wavelength range. Therefore, to compare the results of bacterial viability reduction depending on the light wavelength of irradiation, the use of alternating 525 nm and 660 nm light irradiation would be valuable in further *in vivo* studies.

In light of the latest results presented by Dobrucka and Dlugaszewska, Au–NPs can have an antimicrobial effect *per se*.[46,47] The minimum concentration confirmed by the authors to be bactericidal was 6 μg/ml of Au–NPs against *S. aureus*. By using light-activated Au–NRs, they managed to maintain the bactericidal activity while using a thousand times lower concentration of the formulation. The potential synergistic effect allowed the use of an exceptionally low concentration of the tested systems. The activity of the physical mixtures of Au–NRs@SiO_2 or Au–NRs@PEG–SH with Pheide *a* was maintained even at the NRs and PS concentration of $1.33 \cdot 10^{-13}$ M (Figure 8b) and $1.65 \cdot 10^{-8}$ M (Figure 8a), respectively. Considering the clinical usefulness of PACT, decrease in the concentration of the formulation reduces the risk of systemic adverse effects. In addition, Au–NPs may not only have a photodynamic effect but may also have a complementary photothermal effect. However, the nature of gold's antimicrobial activity has not been fully investigated yet.[1] Silvero *et al.* have compared the antibacterial activity of Au–NPs exposed to light at a wavelength of 525 nm *vs.* those of the samples kept in the dark.[48] Their study shows clear differences in the mechanism of action. According to the results of the TEM analysis, the Au–NPs completely surrounded the bacterial cell. The close adherence of the nanoparticles to the bacteria can justify electrostatic attraction. The membrane of *S. aureus* is negatively charged, while Au–NPs tend to be positively charged. Such a close interaction between the nanoparticles and the bacterial wall allows the photothermal effect to occur. In the case of the nanoparticles proposed in this trial, exposed to a wavelength of 525 nm, a strong activity was only observed at the concentration of $6.66 \cdot 10^{-11}$ M (Figure 8a). This may indicate that the thermal effect dominates, with a lower bactericidal potential than the photodynamic activity. This mechanism is possible thanks to the plasmon effect.[48] The maximum achieved antimicrobial activity of the Au–NPs developed by Silverio *et al.* was a 3 log reduction of bacterial growth under the influence of light.[48] Comparing the data on activity of Au–NPs obtained by Silvero *et al.* with those presented in this paper, it can be concluded that Au–NRs@SiO_2 or Au–NRs@PEG–SH (at a concentration of $6.0 \cdot 10^{-11}$, Figure 8a) are much more efficient, as the activity of the nanorods brings over 5 log reduction. This

Research Article
doi.org/10.1002/ejic.202300668

difference may indicate that the modified AuNRs are much more efficient in transferring the thermal energy to the anchored bacteria, thereby causing potential micro-damage in the bacterial walls that facilitate PS penetration. Gil-Tomas *et al.* have investigated the activity of Au–NPs conjugates with chlorin e6 and glutathione against *S. aureus*, MRSA and *S. pyogenes*.[49] The maximum bactericidal effect achieved was only a 2 log reduction in bacterial growth at the conjugates concentration of $2.88 \cdot 10^{-8}$ M. The authors observed an undeniable synergistic effect between the NPs and the dye, expressed in the reduction of the minimum bactericidal concentration of their mixture.[49] The results presented here were obtained for the concentration of modified Au–NPs and the dye in the physical mixtures of almost two thousand times lower than that in the study presented by the Gil-Thomas group, while the activity we obtained was twice higher. From the point of view of potential applications, the use of Au–NPs in minimal concentrations appears to be extremely beneficial. In 2001, gold was voted Contact Allergen of the Year, although to this day the nature of allergic reactions to gold is at least controversial.[50] Nevertheless, the use of the lowest possible concentration of Au–NPs (a trace element in the human body) is desirable. Another approach concerning the use of Au–NPs against bacteria has been reported by Tawfik *et al.* They studied the activity of Au–NPs modified with methylene blue against *S. aureus*. A formulation containing MB at the concentration of 10^{-7} mg/ml and Au–NPs at the concentration of 10^{-4} M was irradiated by a 660 nm diode laser with a total fluence rate of 24 J/cm^2. The activation made it possible to achieve a reduction of 97% (<1 log) in the viable bacteria. This result does not predispose the formulation to be a potential bactericide. In the case of the physical mixtures of Au–NRs@SiO_2 and Pheide *a* tested in our study at lower concentrations (Figure 8b), after excitation with light at a wavelength of 660 nm, a significantly higher reduction of viable bacterial cells (about 5 log) was observed compared to the data presented by Tawfik *et al.*[51]

Formulations of Au–NRs with bactericidal activity at the level presented in this study have been reported by Maliszewska *et al.*[52] The designed Au–NRs–MB conjugates showed over 3 times higher activity than MB alone. The maximum reduction that could be achieved was 4.7 log. An important issue was the high dark toxicity of the proposed PS.[52] In comparison, the dark toxicity of Au–NRs@SiO_2, Au–NRs@PEG–SH, and their physical mixtures with Pheide *a* presented here is negligible (Figure 8a). The absence of dark toxicity is a desirable property in the case of preparations with a selective bactericidal action. At the same time, it increases the chances of using the proposed formulations in clinical practice.

Conclusions

The synthesis of Au–NRs was carried out by a *seed-mediated growth* process. The functionalization process of Au–NRs was performed with SiO_2 and PEG–SH with different chain lengths (2k, 5k, 10k). Pheide *a*, characterized by the high efficiency of ϕ_Δ, was chosen for this study because this parameter is the most important photophysical factor determining the photodynamic potential and ability to affect biological structures. A series of physical mixtures was prepared, containing a constant concentration of the dye and variable concentrations of Au–NRs. The increase in the intensity of the absorption band in region 660 nm is the result of the increased concentration of Au–NRs in each successive mixture. The light absorption spectra of the tested mixtures are characterized by two different absorption bands of the electromagnetic wave, at 410 nm and 667 nm, from the Soret band and the Q band, respectively. The decreasing intensity of the fluorescence band results from the increasing concentration of Au–NRs in each successive mixture. Linear Stern-Volmer relationships were obtained for all the mixtures tested, which is suggestive of a single quenching mechanism. The most efficient ϕ_Δ, of 65%, was observed for the mixture of Au–NRs@PEG–SH (10k) – Pheide *a*. In order to evaluate the biological activity of the systems studied, the antimicrobial effects against *S. aureus* of pure dye (Pheide *a*) and of its mixture with coated Au–NRs (Au–NRs@SiO_2 or Au–NRs@PEG–SH) were checked. From among the systems studied, the highest activity was observed upon excitation at 660 nm of the physical mixture Au–NRs@PEG–SH (10k) with Pheide *a* at the concentration of $1.33 \cdot 10^{-13}$ M and $1.65 \cdot 10^{-8}$ M, respectively. The bactericidal activity of this mixture exceeded a 5.8 log reduction in bacterial growth ($>$99.999% reduction). Slightly lower but still high activity was obtained with Pheide *a* (around 5 log) and the physical mixtures of Au–NRs@SiO_2 with Pheide *a* at the concentration of $1.33 \cdot 10^{-13}$ M and $1.65 \cdot 10^{-8}$ M, respectively. The results obtained predestine these systems to be excellent candidates for use in medical applications.

Experimental Section

Chemicals

Tetrachloroauric acid ($HAuCl_4 \cdot H_2O$) (99.99%) from Alfa Aesar, cetyltrimethylammonium bromide (CTAB) (99.00%), sodium borohydride ($NaBH_4$) (98.00%), silver nitrate ($AgNO_3$) (99.99%), ascorbic acid (99.00%), sodium hydroxide (99.99%), tetraethylorthosilicate (TEOS) (99.99%), O-(2-mercaptoethyl)-O′-methylpolyethylene glycol (PEG–SH $M_w \approx 2000$ (2k), O-[2-(3-mercaptopropionylamino)ethyl]-O′-methylpolyethylene glycol (PEG–SH $M_w \approx 5000$ (5k)) (99.99%) and O-(2-mercaptoethyl)-O′-methylpolyethylene glycol (PEG–SH $M_w \approx 10000$ (10k)) (99.99%) and 1,3-diphenylobensofuran (DPBF) were purchased from Sigma Aldrich. Ethanol (EtOH) 99.80% H_2O-free was purchased from POCH S.A. (Poland). Pheophorbide *a* (Pheide *a*) ($>$95.00%) was commercially purchased from Frontier Scientific, Inc. (USA).

Chemical synthesis of gold nanorods (Au–NRs)

Prior to the synthesis process of gold nanorods (Au–NRs), aqua regia (HCl:HNO_3 3:1 v/v) was used to treat the glass. Ultrapure water (Milli-Q, 18.2 MΩ·cm, 71.98 ± 0.01 mN·m^{-1}) was used throughout the synthesis process. Au–NRs were prepared according to the procedure of Nikoobakth *et al.*[53] with the modifications previously described by Błaszkiewicz *et al.*.[28] The synthesis of the Au–NRs was carried out by *in situ bottom-up* method involving the reduction of $HAuCl_4$ with $NaBH_4$ in a two-step process. The Au–NRs

were synthesized by the *seed-mediated growth* method, in which the gold particles are attached to the previously obtained spherical gold nanostructures for the production of Au–NRs. A transparent solution is obtained by dissolving CTAB (5 mL, 0.2 M) surfactant in deionized water, then the precursor ($HAuCl_4$) (5 mL, 0.5 mM) and the cooled reducing agent ($NaBH_4$) (0.6 mL, 0.01 M) are added. The solution is brownish-yellow after intensive stirring. The reaction is carried out under sterile conditions by maintaining the temperature and humidity at a constant level. The spherical gold NPs (seed solution) prepared in this way were stored at a temperature of approx. 28 °C, which prevented the crystallization of the CTAB surfactant. Subsequently, 12 μL of the seed solution was added to the growth solution containing CTAB (5 mL, 0.2 M), $HAuCl_4$ (5 mL, 0.001 M), $AgNO_3$ (0.05–0.3 mL, 0.004 M) and ascorbic acid (70 μL, 0.078 M). The growth process takes place when the seed solution is added at a temperature of 27–30 °C. After stirring, the growth solution changed color, indicating the formation of Au–NRs. During the synthesis process, modifications were made, e.g. the water was cooled for the preparation of $NaBH_4$, the gold seeds were stored at 28 °C, and the appropriate concentration of $AgNO_3$ was determined to allow precise control of the size of the Au–NRs. At the end of the synthesis process, the reaction product was properly fractionated and purified by centrifugation and removal of the supernatant.

The functionalization of Au–NRs with PEG–SH (Au–NRs@PEG–SH) was carried out according to the modified method described previously.[29,54] The prepared PEG–SH was added drop by drop under a sonication procedure. The reaction mixture was allowed to stand overnight under mild stirring conditions. After that, the unbound PEG–SH molecules were removed by centrifugation, the supernatant was discarded and the precipitate containing Au–NRs was dispersed in milli-Q water. The amount of PEG–SH (2k, 5k and 10k) required to stabilize the surface of the Au–NRs was calculated according to Manson *et al.*[55] The functionalization of Au–NRs with SiO_2 (Au–NRs@SiO_2) was carried out using the modified method proposed by the Liz-Marzán group[56] with our slight modifications.[28,30] The concentration of the CTAB surfactant must be controlled throughout the reaction process and tetraethyl orthosilicate solution (TEOS) was used for functionalization. The hydrolysis and condensation of TEOS to form SiO_2 can be catalyzed by changing the pH. An 0.1 M NaOH solution was added to the Au–NRs to adjust the pH to approximately 10, and the solutions were stirred for 30 min. Subsequently, TEOS (90 μl of 20% in ethanol) was added dropwise and stirred overnight at room temperature. The Au–NRs were transferred and purified by centrifuging twice for 30 minutes. The supernatant was removed, and the Au–NRs were transferred to ethanol for further processing. During the functionalization, some process modifications were made: after centrifugation and purification of the Au–NRs, the surfactant was added again in appropriate concentrations to control the silica growth process, the pH value was monitored throughout the process, the solvent for the silane was also modified, and the transfer of the Au–NRs to ethanol was performed after prior fractionation and purification by centrifugation and removal of the supernatant.

Microscopic and spectroscopic studies

The morphology and size dispersion of Au–NRs were characterized by transmission electron microscopy (HR-TEM) using a JEOL ARM-200F instrument (200 kV) and JEOL 1400 (120 kV). Au–NRs were drop-casted on Cu grids and placed on a vacuum desiccator overnight.

In the physical mixtures with Pheide *a*, the concentrations of Au–NRs@SiO_2 and Au–NRs@PEG–SH were (0, 1.33, 4.00, 6.66)·10^{-11} M (extinction coefficient 3.11·10^9 $M^{-1}cm^{-1}$[26]), while the concentration of Pheide *a* was set to 1.65·10^{-6} M. Pheide is not covalently bound to the nanoparticle surface, the suspensions are a physical mixture of chemically non-interacting components. The absorption spectra were measured using a Varian Cary 4000 spectrometer. The fluorescent spectra were collected using a Hitachi F4500 fluorometer. All the samples were stirred before and after each collection of spectra. The quantum yield of fluorescence (ϕ_F) of Pheide *a* in the physical mixtures was calculated by the comparative method according to equation (1):

$$\phi_F = \phi_{Ref}\frac{F_S}{F_{Ref}}\frac{1-10^{-A_{Ref}}}{1-10^{-A}}\frac{n^2}{n_{Ref}^2}, \quad (1)$$

where: F_S and F_{Ref} are the areas under the fluorescence emission spectra of the samples and the reference, respectively; A and A_{Ref} are the absorbances of the investigated sample and the references at the excitation wavelength; n and n_{Ref} are the refractive indices of EtOH. The reference was Pheide *a* dye ($\phi_{Ref} = 28\,\%$) dissolved in EtOH.[32]

The process of fluorescence quenching of Pheide *a versus* Au–NRs concentration ($[\boldsymbol{Au-NRs}]$) can be described by the Stern-Volmer constant ($\boldsymbol{K_{SV}}$) defined by the expression:

$$\frac{F_0}{F} - 1 = K_{SV}[Au-NRs], \quad (2)$$

where $\boldsymbol{F_0}$, and $\boldsymbol{F}$, are intensities at the maximum of the fluorescence spectra of Pheide *a* in the absence and in the presence of a quencher (Au–NRs), respectively.[57]

The efficiency of the singlet oxygen generation (ϕ_Δ) was evaluated by using a photometric method based on the absorbance of DPBF, which is widely used as a $^1O_2$ trap. $^1O_2$ was detected *via* the photodegradation of DPBF, which readily undergoes a 1,4-cycloaddition in reaction with $^1O_2$ to form endoperoxides that irreversibly yield 1,2-dibenzoylbenzene.[33,35] For the estimation ϕ_Δ, Pheide *a* dissolved in EtOH was used as a reference.[32] The mixtures of the investigated (or reference) sample were irradiated with monochromatic light using a 1200 W lamp (Oriel 66070) and a Carl Zeiss SPM2 monochromator with a 10 nm half-width of the band. The irradiation wavelength (668 nm) was set at the maximum of the Q_y absorption band of Pheide *a*. The DPBF concentration was kept constant at ~0.75·10^{-5} M. The reaction of the DPBF with $^1O_2$ after irradiation was monitored by measuring the absorbance at 411 nm using a StellarNet Inc. Black-Comet-HR and DH-2000BAL Ocean Optics light source and two Ocean Optics high quality optical fibers to collect the absorption spectra. The value of ϕ_Δ was determined according to the equation:

$$\phi_\Delta = \phi_\Delta^{Ref}\frac{k_S}{k_{Ref}}\frac{1-10^{-A_{Ref}(0)}}{1-10^{-A_S(0)}}, \quad (3)$$

where: ϕ_Δ^{Ref} is the $^1O_2$ generation efficiency of the reference, $\boldsymbol{A_S}(0)$, $\boldsymbol{A_{Ref}}(0)$ are the absorbances of the investigated sample and the reference, respectively, at time 0; $\boldsymbol{k_S}$, $\boldsymbol{k_{Ref}}$ are the slopes of the linear semilogarithmic dependencies describing the photobleaching rate of DPBF in the presence of the investigated and reference samples, respectively.[58]

Microbial cultures

The analysis of the antimicrobial activity was carried out according to the procedure previously described by Sobotta *et al.*[59] Briefly: Gram-positive *Staphylococcus aureus* was cultivated in BHI broth

(bioMerieux, France) for 24 h at a constant temperature of 36 ± 1 °C under aerobic conditions. After incubation, the bacteria were centrifuged and harvested (3000 rpm for 15 min) and then resuspended in 10 mM phosphate-buffered saline (PBS, pH = 7.0). Finally, the suspension was diluted with PBS solution by adjusting it to the value of about 1.5 on the McFarland scale.

Dark activity

The prepared bacterial suspension was added to the wells of a 96-well microtiter plate, and then solution of the pure PS (Pheide *a*), Au–NRs@SiO_2, Au–NRs@PEG–SH or their physical mixtures was added to the wells to achieve the final concentrations. Next, each system was incubated in the dark at room temperature on a laboratory shaker (at a speed of 60 rpm) for 30 minutes. At the same time, a control sample was prepared without adding the investigated systems. Following the pre-incubation period, the bacteria were diluted and plated on tryptic soy agar (TSA) plates. The plates were incubated at a constant temperature of 36 ± 1 °C for 24 h, and then the viability of the microorganisms was assessed by counting CFU. Based on the difference in CFU between the test and control samples, the log reduction of viable microorganisms in each sample was determined.

Light-dependent activity

Analogous to the dark activity, the light activity was evaluated. Identically prepared 96-well microtiter plates after pre-incubation were irradiated with high-power LED Mul-tiChip Emitters (60 high-efficiency AlGaAs diode chips, RoithnerLaserTechnik GmbH, Vienna, Austria). The experiment was carried out independently for the irradiation with light at three different wavelengths of 405 nm, 525 nm, and 660 nm. In each of the tests, light with a fixed dose of 100 J/cm^2 was used.

Statistical analysis

The unpaired Student's t-test and the U Mann-Whitney test were used to determine the significance of the differences between groups. A probability value (P) of less than 0.05 was considered to be significantly different. The statistical analysis was carried out using the STATISTICA software, v.13.0.

Acknowledgements

The authors wish to thank Emerson Coy for the TEM images. The authors thank Maciej Michalak for excellent technical support. This research was funded by the National Science Center in Poland by the project 2021/41/N/ST4/03017 (P.B.) and by the Ministry of Education and Science (0512/SBAD/2320) (A.D.).

Conflict of Interests

The authors declare no conflict of interest.

Data Availability Statement

The data that support the findings of this study are available from the corresponding author upon reasonable request.

Keywords: nanoparticles · noble metal surface plasmon resonance · photodynamic antimicrobial chemotherapy · singlet oxygen generation;

[1] A. Glowacka-Sobotta, D. Ziental, L. Sobotta, in *Appl. Porphyrinoids Funct. Mater.* (Eds.: H. Lang, T. Rueffer), Royal Society Of Chemistry, Cambridge, **2021**, pp. 352–404.
[2] L. Sobotta, P. Skupin-Mrugalska, J. Piskorz, J. Mielcarek, *Dyes Pigm.* **2019**, *163*, 337–355.
[3] L. Sobotta, P. Skupin-Mrugalska, J. Piskorz, J. Mielcarek, *Eur. J. Med. Chem.* **2019**, *175*, 72–106.
[4] L. Sobotta, P. Skupin-Mrugalska, J. Mielcarek, T. Goslinski, J. Balzarini, *Mini-Rev. Med. Chem.* **2015**, *15*, 1–1.
[5] D. Ziental, D. T. Mlynarczyk, B. Czarczynska-Goslinska, K. Lewandowski, L. Sobotta, *Nanomaterials* **2021**, *11*, 2883.
[6] M. Wysocki, B. Czarczynska-Goslinska, D. Ziental, M. Michalak, E. Güzel, L. Sobotta, *ChemMedChem* **2022**, *17*, DOI 10.1002/cmdc.202200185.
[7] K. Granados-Tavera, M. Zambrano-Angulo, N. Montenegro-Pohlhammer, G. Yaşa Atmaca, L. Sobotta, E. Güzel, G. Cárdenas-Jirón, A. Erdoğmuş, A. G. Gürek, *Dyes Pigm.* **2023**, *210*, 110986.
[8] P. Błaszkiewicz, M. Kotkowiak, *Curr. Med. Chem.* **2018**, *25*, 5914–5929.
[9] P. Skupin-Mrugalska, L. Sobotta, A. Warowicka, B. Wereszczynska, T. Zalewski, P. Gierlich, M. Jarek, G. Nowaczyk, M. Kempka, J. Gapinski, S. Jurga, J. Mielcarek, *J. Inorg. Biochem.* **2018**, *180*, 1–14.
[10] P. Skupin-Mrugalska, J. Piskorz, T. Goslinski, J. Mielcarek, K. Konopka, N. Düzgüneş, *Drug Discovery Today* **2013**, *18*, 776–784.
[11] Y. Cheng, A. C. Samia, J. D. Meyers, I. Panagopoulos, B. Fei, C. Burda, *J. Am. Chem. Soc.* **2008**, *130*, 10643–10647.
[12] M. Pola, H. Kolarova, R. Bajgar, *J. Med. Sci.* **2022**, *91*, e752.
[13] L. A. Dykman, N. G. Khlebtsov, *Biomaterials* **2016**, *108*, 13–34.
[14] F. Schulz, W. Friedrich, K. Hoppe, T. Vossmeyer, H. Weller, H. Lange, *Nanoscale* **2016**, *8*, 7296–7308.
[15] Z. Zhang, M. Lin, *RSC Adv.* **2014**, *4*, 17760–17767.
[16] A. A. Glowacka-Sobotta, B. D. Ziental, C. L. Sobotta, in *Appl. Porphyrinoids Funct. Mater.*, The Royal Society Of Chemistry, **2021**, pp. 352–404.
[17] F. Rossi, N. T. K. Thanh, X. D. Su, *ACS Appl. Bio Mater.* **2019**, *2*, 3059–3067.
[18] M. Okkeh, N. Bloise, E. Restivo, L. De Vita, P. Pallavicini, L. Visai, *Nanomaterials* **2021**, *11*, 312.
[19] "Photobactericidal activity activated by thiolated gold nanoclusters at low flux levels of white light | Nature Communications," can be found under https://www.nature.com/articles/s41467-020-15004-6, **n.d.**
[20] F. Lavaee, M. Motamedifar, G. Rafiee, *Lasers Med. Sci.* **2022**, *37*, 1717–1725.
[21] I. Maliszewska, E. Wanarska, A. C. Thompson, I. D. W. Samuel, K. Matczyszyn, *Molecules* **2021**, *26*, 623.
[22] K. Rahme, L. Chen, R. G. Hobbs, M. A. Morris, C. O'Driscoll, J. D. Holmes, *RSC Adv.* **2013**, *3*, 6085–6094.
[23] D. C. Hone, P. I. Walker, R. Evans-Gowing, S. FitzGerald, A. Beeby, I. Chambrier, M. J. Cook, D. A. Russell, *Langmuir* **2002**, *18*, 2985–2987.
[24] O. Planas, N. Macia, S. Nonell, B. Heyne, *J. Am. Chem. Soc.* **2016**, *138*, 2762–2768.
[25] N. Macia, V. Kabanov, M. Côté-Cyr, B. Heyne, *J. Phys. Chem. Lett.* **2019**, *10*, 3654–3660.
[26] C. J. Orendorff, C. J. Murphy, *J. Mater. Chem. B* **2006**, *110*, 3990–3994.
[27] L. Scarabelli, A. Sánchez-Iglesias, J. Pérez-Juste, L. M. Liz-Marzán, *J. Phys. Chem. Lett.* **2015**, *6*, 4270–4279.
[28] P. Błaszkiewicz, M. Kotkowiak, E. Coy, A. Dudkowiak, *J. Phys. Chem. C* **2020**, *124*, 2088–2095.
[29] X. Du, W. C. Lin, Q. Shou, X. Liang, H. Liu, *Colloid Polym. Sci.* **2019**, *297*, 891–902.
[30] P. Błaszkiewicz, M. Kotkowiak, E. Coy, A. Dudkowiak, *J. Phys. Chem. C* **2019**, *123*, 27181–27186.
[31] B. Tim, P. Błaszkiewicz, M. Kotkowiak, *J. Mol. Liq.* **2022**, *349*, 118179.
[32] M. Kotkowiak, A. Dudkowiak, *Phys. Chem. Chem. Phys.* **2015**, *17*, 27366–27372.

[33] S. J. Chadwick, D. Salah, P. M. Livesey, M. Brust, M. Volk, *J. Phys. Chem. C* **2016**, *120*, 10647–10657.
[34] L. Liu, X. Luo, J. Liu, *Small* **2020**, *16*, 2000011.
[35] X. Ke, D. Wang, C. Chen, A. Yang, Y. Han, L. Ren, D. Li, H. Wang, *Nanoscale Res. Lett.* **2014**, *9*, 1–8.
[36] D. M. Bamberger, S. E. Boyd, *Am. Fam. Physician* **2005**, *72*, 2474–2481.
[37] J. Kluytmans, M. Struelens, *BMJ* **2009**, *338*, b364.
[38] C. L. Ventola,P T **2015**, *40*, 277–283.
[39] M. Frieri, K. Kumar, A. Boutin, *J. Infect. Public Health* **2017**, *10*, 369–378.
[40] A. Kawczyk-Krupka, B. Pucelik, A. Międzybrodzka, A. R. Sieroń, J. M. Dąbrowski, *Photodiagn. Photodyn. Ther.* **2018**, *23*, 132–143.
[41] M. Wysocki, D. Ziental, M. Jozkowiak, J. Dlugaszewska, H. Piotrowska-Kempisty, E. Güzel, L. Sobotta, *Synth. Met.* **2023**, *299*, 117474.
[42] "Light Sources and Dosimetry Techniques for Photodynamic Therapy - Kim - 2020 - Photochemistry and Photobiology - Wiley Online Library," can be found under https://onlinelibrary.wiley.com/doi/10.1111/php.13219, **n.d.**
[43] G. Jori, C. Fabris, M. Soncin, S. Ferro, O. Coppellotti, D. Dei, L. Fantetti, G. Chiti, G. Roncucci, *Lasers Surg. Med.* **2006**, *38*, 468–481.
[44] A. Schrier, G. Greebel, H. Attia, S. Trokel, E. F. Smith, *J. Refract. Surg.* n.d., *25*, DOI 10.3928/1081597X-20090813-07.
[45] T. L. de Jager, A. E. Cockrell, S. S. Du Plessis, in *Ultrav. Light Hum. Health Dis. Environ.* (Ed.: S. I. Ahmad), Springer International Publishing, Cham, **2017**, pp. 15–23.
[46] R. Dobrucka, J. Dlugaszewska, *Inorg. Nano-Met. Chem.* **2020**, *50*, 459–468.
[47] R. Dobrucka, J. Długaszewska, M. Kaczmarek, *Arab. J. Chem.* **2016**, *12*, DOI 10.1016/j.arabjc.2016.02.009.
[48] M. J. Silvero, G. A. Argüello, M. C. Becerra, *J. Nanopharm. Drug. Deliv.* **2014**, *2*, 148–152.
[49] J. Gil-Tomás, L. Dekker, N. Narband, I. P. Parkin, S. P. Nair, C. Street, M. Wilson, *J. Mater. Chem.* **2011**, *21*, 4189.
[50] J. K. Chen, H. P. Lampel, *Dermatitis* **2015**, *26*, 69–77.
[51] A. A. Tawfik, J. Alsharnoubi, M. Morsy, *Photodiagn. Photodyn. Ther.* **2015**, *12*, 215–220.
[52] I. Maliszewska, A. Leśniewska, J. Olesiak-Bańska, K. Matczyszyn, M. Samoć, *J. Nanopart. Res.* **2014**, *16*, 2457.
[53] B. Nikoobakht, M. A. El-sayed, *Chem. Mater.* **2003**, 15, 1957–1962.
[54] P. Szustakiewicz, N. Kolsut, A. Leniart, W. Lewandowski, *Nanomaterials* **2019**, *9*, 1–16.
[55] J. Manson, D. Kumar, B. J. Meenan, D. Dixon, *Gold Bull.* **2011**, *44*, 99–105.
[56] L. M. Liz-Marzán, M. Giersig, P. Mulvaney, *Langmuir* **1996**, *12*, 4329–4335.
[57] N. J. B. Green, S. M. Pimblott, M. Tachiya, *J. Phys. Chem.* **1993**, *97*, 196–202.
[58] R. T. Aroso, M. J. F. Calvete, B. Pucelik, G. Dubin, L. G. Arnaut, M. M. Pereira, J. M. Dąbrowski, *Eur. J. Med. Chem.* **2019**, *184*, 111740.
[59] L. Sobotta, D. Ziental, J. Sniechowska, J. Dlugaszewska, M. J. Potrzebowski, *Photochem. Photobiol. Sci.* **2019**, *18*, 213–223.

Manuscript received: November 18, 2023
Revised manuscript received: December 23, 2023
Accepted manuscript online: February 15, 2024
Version of record online: March 5, 2024

Correction added on 26.3.2024: Correction in author affiliation